Applied Catalysis B: Environmental 282 (2021) 119515

Contents lists available at ScienceDirect

Applied Catalysis B: Environmental

journal homepage: www.elsevier.com/locate/apcatb

Ru on N-doped carbon supports for the direct hydrogenation of cellobiose into sorbitol

Samuel Carlier, Jim Gripekoven, Martin Philippo, Sophie Hermans*

Université catholique de Louvain, IMCN Institute, Place L. Pasteur 1, 1348 Louvain-la-Neuve, Belgium

ARTICLE INFO

Keywords:
Biomass conversion
Cellulose
Cellobiose
Nitrogen doping
Carbon
Graphene nanoplatelets
Sorbitol
Ruthenium

ABSTRACT

With the aim to produce the platform molecule sorbitol from biomass, the two-steps transformation of the cellobiose disaccharide by hydrogenation/hydrolysis was attempted using a single catalytic material. The two reactions were first studied separately before integration. Ru nanoparticles deposited on carbon supports were tested for the hydrogenation of glucose into sorbitol. The optimal nanoparticles size was established. Two different types of carbon materials (activated coal and graphene nanoplatelets) were modified to incorporate nitrogen atoms within the carbon lattice. These N-doped carbon materials displayed higher basicity but showed no activity for the hydrolysis of cellobiose into glucose. They were used to support Ru nanoparticles and these bifunctional catalysts were studied for the hydrogenolysis of cellobiose into sorbitol. Kinetic studies showed that the doping of the carbon supports increased the activity of the Ru nanoparticles for this reaction, going through a hydrogenation followed by disaccharide splitting pathway rather than vice versa. Catalysts were reused and no sign of deactivation have been observed.

1. Introduction

Today the increasing energy demand and depletion of fossil fuel reserves have motivated the utilization of biomass resources to produce fuels and chemicals as a renewable and sustainable alternative [1]. Lignocellulosic biomass, which is composed of lignin (15–35 %), hemicellulose (25–35 %) and cellulose (40–50 %), is the most abundant biomass type and its non-edible feature makes it very attractive for further transformation [2,3]. Cellulose is a polymer of glucose connected by β-1,4-glycosidic bonds. Cellulose has high crystallinity due to intermolecular and intramolecular hydrogen bonds. For this reason, it is not soluble in most solvents [4]. Usually, the first step for upgrading it involves hydrolysis into constituting sugar units. The main known processes for cellulose hydrolysis are the use of mineral acids (e.g., H_2SO_4) [1,5], acidic solid catalysts (Amberlyst, sulfonated carbons) [6–9] or supercritical water [10] and ionic liquids [11]. The main interest behind these studies of cellulose depolymerization is to obtain glucose. Glucose can further be transformed into platform or building block molecules such as 5-hydroxymethylfurfural, ethylene glycol, gluconic acid or sorbitol [12]. Sorbitol is a very useful molecule. It can be used as precursor in food and pharmaceutical industry. Moreover it is a chemical platform that can lead to molecules such as sorbitan, isosorbide, glycerol, *etc*. [13].

Cellobiose which is composed of only two glucose units bound together by the β-1,4-glycosidic bond is the simplest model for cellulose and will be used in this study. It has been pointed out that two reaction pathways can occur for the transformation of cellobiose into sorbitol, also called hydrogenolysis (Scheme 1) [14,15]. In the first pathway, cellobiose is hydrolyzed into glucose before being hydrogenated into sorbitol. In the second pathway, cellobiose is first hydrogenated into cellobitol (another disaccharide) and cellobitol is then hydrolyzed into one molecule of sorbitol and one molecule of glucose, which can further be hydrogenated into sorbitol.

The direct catalytic conversion of cellulose into sorbitol has been achieved [16] but remains very challenging. Efficient and selective catalytic systems need to be investigated. The hydrogenation of cellulose into sorbitol necessitates two main components: noble metals nanoparticles like Pt, Pd, or Ru for redox activity and acid species (usually soluble mineral acids or heteropolyacids) to break the β-1,4-glycosidic bond. Heterogeneous catalysts are presently the most studied for this reaction. Metal nanoparticles are usually deposited on a support displaying acidic properties. Inorganic oxides such as SiO_2 [17] or even Al_2O_3 [18] are often used. Zeolites such as ZSM-5 [19], Beta [20] or USY [4] have been investigated as well. Zeolites have strong Brönsted acid sites but have poor hydrothermal stability [21]. Some resins, like Amberlyst, which display high acidity have been used as a support for

* Corresponding author.
E-mail address: sophie.hermans@uclouvain.be (S. Hermans).

https://doi.org/10.1016/j.apcatb.2020.119515
Received 30 June 2020; Received in revised form 28 August 2020; Accepted 30 August 2020
Available online 06 September 2020
0926-3373/

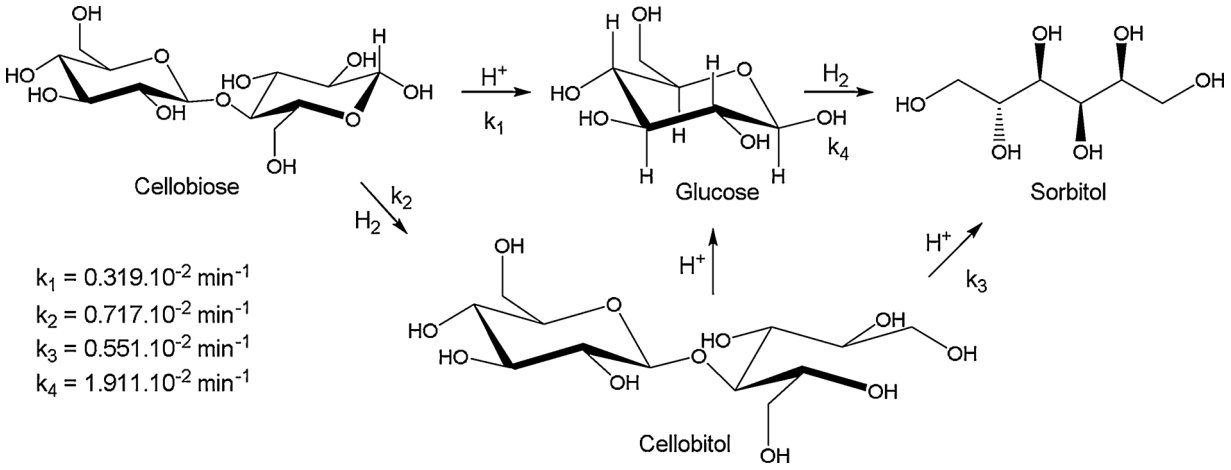

Scheme 1. Two different pathways for the transformation of cellobiose into sorbitol (reaction rate constants were taken from the literature [14]).

Ru nanoparticles [8]. Activated carbons and nanotubes that have been treated to increase acidity with SO_3H or COOH functions have shown interesting results [22,23].

Currently, many studies try to improve the hydrolysis step of this transformation by designing new acidic catalysts. However, improving the Ru activity can also be an interesting approach. Indeed, this would activate the second reaction route (bottom in Fig. 1) by hydrogenating the disaccharide before breaking it. It has indeed been shown that hydrolysis of cellobitol is faster than the hydrolysis of cellobiose [14]. In the present study, we aim at optimizing the high hydrogenation activity of Ru/C for this transformation without any acidity from the support or the solution. The optimal Ru nanoparticles size on the chosen carbon supports will be identified. Moreover, we will determine the preferential pathway of this reaction and highlight the improvement of Ru activity over N-doped carbon supports with kinetic studies. Indeed, it is known that nitrogen atoms introduced within the lattice of carbon materials can influence the activity of metallic nanoparticles deposited on it [24]. Eventually, recyclability tests have been carried out to assess the stability and reusability of the catalysts.

2. Experimental

2.1. Reagents and materials

The activated carbon (AC; SX + type) (Boehm acidity: 42 mmol/100 g) was obtained from NORIT. The carbon nanofibers (CNF; LHT and LHT-OX type) (Boehm acidity: 10 mmol/100 g) were obtained from Applied Sciences Inc (USA). The graphene nanoplatelets (GNP; C750 type) were purchased from Sigma-Aldrich. Thionyl chloride, ethylenediamine, D-(+)-cellobiose (≥99 %) were also supplied by Sigma-Aldrich and used as received.

2.2. Nitrogen doping

1 or 2 g of support was dispersed in respectively, 100 mL or 200 mL of HNO_3 solution (2.5 mol/L) in a three-neck round-bottom flask. The suspension was then heated under reflux and agitation at 105 °C. After 24 h, the mixture was filtrated on a Büchner and extensively washed with water until constant pH. Finally, the resulting solid was oven dried overnight at 100 °C.

The oxidized support was dispersed in 100 mL of toluene in a three-neck round-bottom flask. 6 mL of pure thionyl chloride were then added using a 12 mL syringe and the suspension was heated under reflux and agitation at 110 °C. After 5 h, the mixture was filtrated and extensively washed with 500 mL of toluene. The resulting solid was then oven dried overnight at 100 °C.

The chlorinated support was dispersed in a mixture of 70 mL toluene and 30 mL ethylenediamine in a three-neck round-bottom ask. The suspension was then heated under reflux and agitation at 110 °C. After 24 h, the mixture was filtrated and washed extensively with ethanol. The resulting solid was then oven dried overnight at 100 °C.

The solid was then heat-treated in a furnace (Carbolite STF 16/-/450) under inert atmosphere (N2) following the temperature program below:

a Temperature rising at 100 °C/h to the desired temperature (700 °C/900 °C).
b Two hours plateau at the desired temperature.
c Temperature decrease at 100 °C/h to room temperature.

2.3. Ru nanoparticles deposition

150 mg of urea was dissolved in 100 mL of a water dispersion containing 250 mg of support. As 3 wt% of Ru loading on the support is targeted, 18.4 mg of RuCl3 (Sigma Aldrich) was then added. After one hour stirring, the heating was turned on to 120 °C (urea starts to decompose at 90 °C) and the solution remained at this temperature for one hour before cooling down. Then, at room temperature, 2 g of sodium formate were added and the solution was left under agitation for one hour. After that, the solution was set to 130 °C (formate degradation temperature) for one hour. Then, the solution was left at room temperature under agitation overnight. Following this, the solid was filtrated out, washed extensively with water and oven dried overnight. Finally, the solid was heat-treated under reductive atmosphere in order to obtain the desired particles size (Alphagaz mix: 5 % H_2 / 95 % Ar) at 400 °C or 600 °C for two hours with the same temperature program used for the nitrogen doping, as described above.

2.4. Catalytic tests

The tests were carried out in a 250 mL stainless steel Parr autoclave. 1 g of cellobiose was added to either 20 mg of catalyst for hydrogenation test or 150 mg of catalyst for hydrolysis test in 120 mL of mQ water. These testing conditions were based on precedents in the literature [25,26]. The low cellobiose concentration ensures absence of diffusional limitations. Then, the autoclave was sealed and the system was purged three times with nitrogen and heated up to 120 °C or 160 °C under autogenic pressure of N_2 for the hydrolysis tests and under 30 bar of H_2 for the hydrogenation tests (this pressure is set when the temperature of 160 °C is reached). At that controlled temperature, the agitation was started at 1700 rpm for several hours. After this fixed duration of catalytic test, the system was then cooled down to room

temperature and the solution was filtrated. The solid catalyst was washed and dried. The filtrate was then diluted to 250 mL with mQ water and analyzed by HPLC. For hydrolysis test on cellobiose, the same conditions were used except the reaction was carried out under autogenic N_2 pressure and at 160 °C. For kinetic studies, at various time intervals, liquid samples were taken and two times diluted with mQ water before analyzing it similarly. The pressure within the autoclave was brought back to 30 bar of H_2 after each sampling.

HPLC analyses were performed with a Waters system equipped with Waters 2414 refractive index (RI) detector (detector temperature = 30 °C). Two columns were used. The first one is a Carbohydrate Transgenomic CarboSep CHO682 column, with mQ H2O (18 MΩ.cm at 25 °C) as eluent, a flux of 0.4 mL/min, a column temperature of 80 °C and 20 µL of injected volume. The second one is an Aminex HPX 87C column, with mQ H2O (18 MΩ.cm at 25 °C) as eluent, a flux of 0.5 mL/min, a column temperature of 85 °C and 25 µL of injected volume.

The conversion of cellobiose was calculated as follows:

$$Cellobiose\ conversion\ (\%) = \frac{n\ cellobiose\ converted}{initial\ n\ cellobiose} * 100$$

The selectivity in glucose was calculated as follows:

$$Selectivity\ in\ glucose\ (\%) = \frac{n\ glucose\ produced}{2\ *(n\ cellobiose\ converted)} * 100$$

The selectivity in sorbitol was calculated as follows:

$$Selectivity\ in\ sorbitol\ (\%) = \frac{n\ sorbitol\ produced}{2\ *(n\ cellobiose\ converted)} * 100$$

The selectivity in cellobitol was calculated as follows:

$$Selectivity\ in\ cellobitol\ (\%) = \frac{n\ cellobitol\ produced}{n\ cellobiose\ converted} * 100$$

The yield in glucose from cellobiose was calculated as follows:

$$Yield\ in\ glucose\ (\%) = \frac{n\ glucose\ produced}{2\ *\ initial\ n\ cellobiose} * 100$$

The yield in sorbitol from glucose was calculated as follows:

$$Yield\ in\ sorbitol\ (\%) = \frac{n\ sorbitol\ produced}{initial\ n\ glucose} * 100$$

The yield in sorbitol from cellobiose was calculated as follows:

$$Yield\ in\ sorbitol\ (\%) = \frac{n\ sorbitol\ produced}{2\ *\ initial\ n\ cellobiose} * 100$$

2.5. Characterization methods

XPS analyses were carried out at room temperature with a SSI-Xprobe (SSX 100/206) photoelectron spectrometer from Surface Science Instruments (USA), equipped with a monochromatized microfocus Al X-ray source. Samples were stuck onto small sample holders with double face adhesive tape and then placed on an insulating ceramic carousel (Macor®, Switzerland). Charge effects were avoided by placing a nickel grid above the samples and using a flood gun set at 8 eV. The binding energies were calculated with respect to the C-(C, H) component of the C1s peak fixed at 284.4 eV. Data treatment was performed using the CasaXPS program (Casa Software Ltd., UK). The peaks were decomposed into a sum of Gaussian/Lorentzian (85/15) after subtraction of a Shirley-type baseline.

TEM analyses have been conducted as follows: the powder samples were suspended in hexane under ultrasonic treatment, then a drop of the supernatant was deposited on a holey carbon film supported on a copper grid (Holey Carbon Film 300 Mesh Cu, Electron Microscopy Sciences) which was dried overnight under vacuum at room temperature before analysis. The images were obtained on a LEO 922 OMEGA energy filter transmission electron microscope.

TPD-CO_2 analyses were performed on Hiden Catlab reactor combined with a QGA Hiden quadrupole mass spectrometer. During the first stage, the sample was heated to 850 °C at 10 °C/min under an inert flux of argon at 50 mL/min. Then, the temperature was maintained for two hours after which it is let to cool down to 60 °C. Carbon dioxide was then injected with argon (CO_2/Ar: 15/85) at 30 mL/min additionally to the first argon inlet. Then comes the second stage: carbon dioxide inlet was stopped and only argon flows at 50 mL/min through the sample at 60 °C for one hour. Next, the sample was heated again from 60 °C to 800 °C at 10 °C/min in flowing argon.

Powder X-ray diffraction (PXRD) patterns were recorded at room temperature on a Siemens D5000 diffractometer equipped with a Ni filter using CuK_α radiation (BraggBrentano geometry) operated at 40 kV and 40 mA. Diffractograms were taken between 5° and 80° (2θ) with a step size of 0.02° (2θ).

Boehm titration method was used to evaluate the catalysts basicity, based on the procedure used for acidity determination but in the opposite way [27,28]. Namely, NaOH solutions were prepared by dilution of Titrisol ampoules (VWR) containing precise and known quantities of sodium hydroxide. HCl solutions were prepared by the dilution of concentrated hydrochloric acid. The HCl concentrations were determined by titration with the standard NaOH solutions. These solutions were prepared with mQ water that had been previously decarbonated by nitrogen flushing. For titrating the basic groups, 60 mg of sample were dispersed in 30 mL of HCl 0.01 mol/L and the solution was decarbonized for one hour under Ar flux. The mixture was then agitated for 23 h under Ar atmosphere. The suspension was then filtrated and two times 10 mL of the resulting filtrate were back-titrated, under Ar flux, using the NaOH 0.005 mol/L solution. The indicator used was phenolphthalein. The amount of basic functions in the catalyst was determined by calculating the difference between the initial amount of HCl engaged and the amount of remaining HCl after 24 h, titrated by the NaOH.

To evaluate ruthenium content, ICP analyses have been conducted. The sample is first burnt to eliminate the carbon that can cause interferences. Then, ruthenium is mineralized by sodium peroxide (Na_2O_2) by ICP method.

Total organic content (TOC) analyses have been performed as such: a TOC L analyzer separates the different forms of carbon by their "purgeability", that is to say the tendency of these substances to leave the solution when they are displaced by a current of gas (sparging technique). Then each fraction is oxidized in an oven at 680 °C and the CO_2, product of combustion, is measured by non-dispersive infrared spectroscopy (NDIR). The concentrations are obtained by comparison with a calibration carried out under strict same conditions from potassium hydrogen phthalate.

3. Results and discussion

In order to obtain efficient catalysts for the targeted two-step process, we first studied the impact of the Ru nanoparticles size on the hydrogenation catalysis step. Then, the supports were doped with nitrogen to evaluate its influence on the hydrolysis step and observe if there is an improvement of the Ru activity for the whole process.

3.1. Hydrogenation of glucose into sorbitol with Ru/C samples

First, Ru nanoparticles have been deposited on carbon nanofibers (LHT and LHT-OX which are simply oxidized LHT) as described in the experimental section in order to assess the optimal nanoparticles size for the transformation of glucose into sorbitol. To do so, first, Ru has been precipitated as hydroxide by urea degradation using deposition-precipitation method [29]. The catalysts have then been reduced under Ar/H_2 (95/5) at different temperatures to promote controlled coalescence and obtain nanoparticles of different sizes. Carbon nanofibers

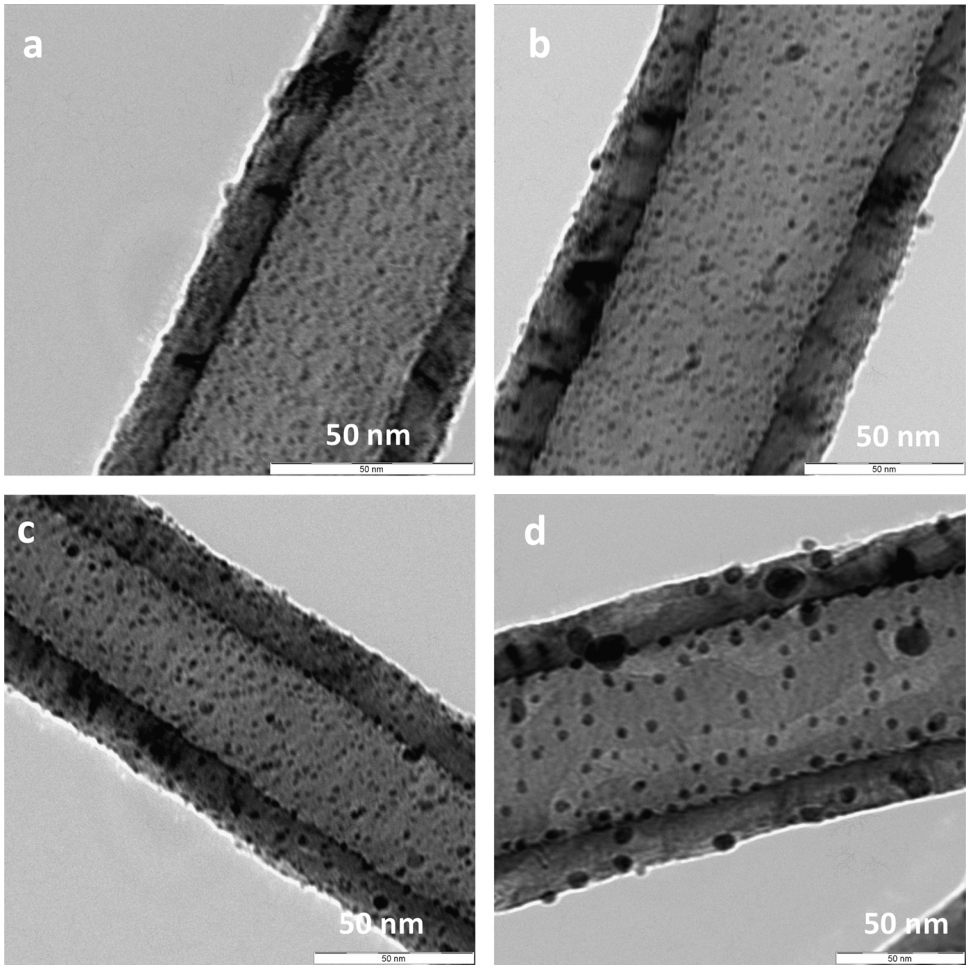

Fig. 1. TEM images of Ru nanoparticles deposited on CNF (LHT-OX) by deposition-precipitation method: (a) without any thermal treatment (b) heated under reductive atmosphere at 600 °C (c) at 900 °C (d) at 1200 °C.

were chosen as model supports because they stabilize small nanoparticles and present a homogeneous carbon surface and structure.

TEM images of the catalysts have been taken and are shown in Fig. 1. Without any heating, the nanoparticles have an average size of less than 1 nm (standard deviation of 0.3 nm) (Fig. 1 (a)). After thermal treatment at 600 °C, the size is growing to 1 – 2 nm (standard deviation of 0.5 nm) (Fig. 1(b)). At 900 °C we obtained nanoparticles between 2 and 5 nm (standard deviation of 1.1 nm) (Fig. 1(c)). Finally at 1200 °C, the nanoparticles size ranges from 5 nm to 10 nm (standard deviation of 1.6 nm) (Fig. 1(d)). Four other catalysts have been synthesized in exactly the same conditions on non-oxidized nanofibers (LHT) for comparison (the corresponding TEM images are given in Electronic Supplementary Material, S1 in SI). It is interesting to note that these carbon nanofibers stabilize very well the nanoparticles. Indeed, even at high temperature, sintering is low and we are keeping relatively small nanoparticles that more importantly remain nicely distributed over the carbon surface. It is known that Ru has not a strong tendency of growing into large particles. But in the literature we can see that Ru nanoparticles of over 10 nm can be obtained after a heat treatment at only 500 °C [22]. The fact that we obtain the same size after a treatment at 1200 °C shows that the CNF are decreasing the sintering phenomena.

These catalysts have been tested in the hydrogenation of glucose into sorbitol. The results are presented in Table 1. First, we observe that Ru is improving both conversion and selectivity towards sorbitol even when it is not reduced before the reaction (because Ru can be reduced in situ during the catalytic test by the H_2 atmosphere). This is concluded based on comparisons with blank test (without any catalyst) and tests involving the bare supports. Second, we notice that the oxidized nanofibers are better supports than the non-oxidized ones. For all nanoparticles sizes, Ru is more active when it is deposited on oxidized nanofibers. Finally, the conversion is different depending on the nanoparticles size and the maximum of sorbitol yield is obtained with Ru/LHT-OX reduced at 600 °C. It means that small nanoparticles are more active for the hydrogenation of glucose into sorbitol and the optimal nanoparticles size is around 1 – 2 nm. We observed (S2 in SI) that there is no link between the activity and the O amount measured by XPS within the samples. The differences of yield can be attributed solely

Table 1
Hydrogenation of glucose into sorbitol at 120 °C under 30 bar of H_2 during 2 h.

Catalyst	Thermal treatment under Ar/H_2 (95/5)	Nanoparticles size (nm)	Glucose conversion (%)	Selectivity in sorbitol (%)	Yield in sorbitol (%)
Blank	/	/	**9**	**41**	**4**
LHT	/	/	**10**	**15**	**2**
Ru / LHT	/	< 1	**40**	**80**	**32**
Ru / LHT	600 °C	1 – 2	**33**	**38**	**13**
Ru / LHT	900 °C	2 – 5	**12**	**81**	**10**
Ru / LHT	1200 °C	5 – 10	**4**	**80**	**3**
LHT-OX	/	/	**14**	**23**	**3**
Ru / LHT-OX	/	< 1	**57**	**78**	**44**
Ru / LHT-OX	600 °C	1 – 2	**74**	**84**	**62**
Ru / LHT-OX	900 °C	2 – 5	**62**	**83**	**51**
Ru / LHT-OX	1200 °C	5 – 10	**14**	**41**	**6**

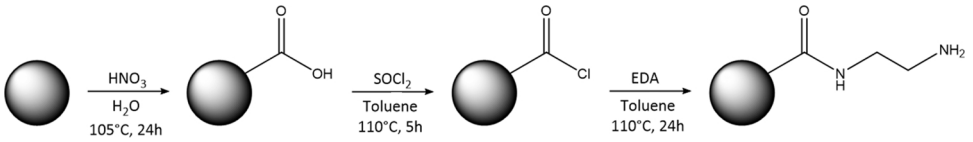

Scheme 2. Functionalization of carbon supports with ethylenediamine.

to the different nanoparticles sizes and not to the removal of some oxygenated functions during heat-treatment.

The same methodology was applied to the two other carbonaceous supports considered in this work, namely activated coal (AC) and graphene nanoplatelets (GNP). Ru was deposited on the solid surface and then heat-treated at different temperatures (TEM images are presented in S3 in SI). The Ru nanoparticles are less visible due to the nature of those supports and the contrast given by their thickness. It has been observed that sintering is higher on AC and GNP than on CNF. Therefore, heat-treatment at 400 °C gives the optimal nanoparticles size of 1 − 2 nm on both AC and GNP (against 600 °C for CNF). This highlights once more the stabilizing effect of the CNF on the Ru nanoparticles.

3.2. N-doped carbon supports synthesis

N-doped carbon supports have been synthesized as described in the experimental section. The first step is a nitric acid oxidation to promote carboxylic group formation on the surface of the carbon support. These carboxylic acid groups are subsequently transformed into acyl chlorides. Then, the chlorine is replaced by ethylenediamine (EDA) (Scheme 2). Finally, the heat treatment will decompose EDA and incorporate the nitrogen atoms in the carbon supports lattice.

The three types of carbon supports were treated this way: carbon nanofibers (CNF LHT-OX), activated coal (AC) and graphene nanoplatelets (GNP). Carbon nanofibers could not be oxidized further with HNO_3, as it is already the oxidized form of CNFs. It can be seen that the O/C ratio measured by XPS is not increased after the oxidation for CNFs whereas it is highly improved after oxidation of AC and GNP (Table 2).

These functionalized materials have also been characterized by Boehm titration and XPS (O/C and N/C ratios) at each step of their preparation (Table 2). Indeed the nitrogen incorporated within the support present a basic character that can be determined by such back-titration method. The quantification of the basic sites can inform us on the amount of nitrogen incorporated in the carbon materials.

Obviously, nitric acid treatment causes a decrease in basicity measured by titration. We notice that, in the next step, the incorporation of EDA is increasing nitrogen content and basicity of the support. After the heat-treatment, these dangling amine functions will mainly be destroyed and a small portion of the nitrogen will be inserted in the structure of the carbon support and form nitrogenated heterocycles. This is witnessed by the decrease of N/C ratio. The increase of basicity after heat-treatment for AC is also explained by the decomposition of oxygenated functions that transform into basic functions such as chromene and pyrone [30]. It is also pointed out that pre-oxidized GNP are more N-functionalized than the pristine GNP even though GNP display more O-group than the other supports at the start (Boehm acidity for pristine GNP: 228 mmol/100 g). The final basicity and the amount of nitrogen are both higher for the pre-oxidized material. This is explained by the need for carboxylic acid functions to attach the EDA on the support (Scheme 2). The amount of nitrogen on the surface of the functionalized carbons determined by XPS analyses, namely the N over C ratio, is varying exactly the same way than the basicity determined by Boehm titration (S4 in SI), confirming the link between the two factors and the incorporation of nitrogen. Strikingly, the final sample of CNFs incorporated very low levels of N and displayed no basicity. This carbon support was therefore discarded for the following steps.

Table 2
Basicity from Boehm titration and atomic ratios determined by XPS for the pristine and the functionalized supports.

Catalysts	Thermal treatment (°C)	O/C atomic ratio (XPS)	Basicity (mmol/100 g)	N/C atomic ratio (XPS)
CNF	/	0.035	0	0.002
Oxidized CNF	/	0.020	0	0.002
EDA-CNF	/	0.026	10	0.017
N-doped CNF	700	0.018	0	0.008
AC	/	0.041	24	0.003
Oxidized AC	/	0.135	5	0.006
EDA-oxidized AC	/	0.160	46	0.111
N-doped oxidized AC	900	0.055	91	0.035
GNP	/	0.063	31	0.000
EDA-GNP	/	0.051	102	0.043
N-doped GNP	900	0.025	61	0.008
Oxidized GNP	/	0.258	0	0.004
EDA-oxidized GNP	/	0.095	167	0.077
N-doped oxidized GNP	900	0.018	81	0.014

Depending on the type of nitrogen functions present on the support, nitrogen peaks (N1s) obtained by XPS analyses will appear at different binding energies. After grafting EDA but before heat-treatment, we have as expected a majority of terminal amine functions (NH_2 peak at 400 eV). After the heat treatment, nitrogen enters within the carbon structure and functions such as pyridine or pyrrole appear, as confirmed by increase of the peak at 398.6 eV in the XPS spectrum of N-doped GNP (Fig. 2). The same observation can be made for N-doped AC (S5 in SI).

We can therefore quantify the amount of pyridine/pyrrole functions versus amine functions. Before heat-treatment, we have almost 80 % of amines functions. After heat treatment, we have less total amount of nitrogen but the ratio between amine functions and pyridine/pyrrole functions is around 50/50 (in at.%).

CO_2-TPD analyses have been carried out on the N-doped supports to confirm the presence of basic sites. The TPD analyses for the N-doped activated coal are presented in Fig. 3. TPD analyses for the N-doped GNPs can be found in the supporting information (S6 in SI).

For the N-doped activated coal, the basicity amounts to 63 mmol/100 g if the first CO_2 desorption peak is considered (starting at 200 °C) together with the main contribution at 750 °C. It is interesting to link this measure to the result obtained by Boehm titration on the same sample (Table 2). Both results are in the same order of magnitude but slightly different (63 vs 91). For GNPs, the difference is more pronounced (21 vs 81) with also a higher figure for basicity measured by Boehm titration. It is important to point out that the amount of CO_2 desorbed variates with the temperature at which the saturation is carried out [31]. At 50 °C, even the weakest sites adsorb the probe molecule that will then be quantified during the desorption. This slight difference could also come from the hypothesis that one CO_2 molecule was adsorbed on each basic site whereas the reality might be that two close basic sites adsorb only one molecule, underestimating the number of basic sites determined by TPD. In addition, the main peak seems to extend above 800 °C, which could not be measured with our instrument. This difference in basicity can also be the result of the short pre-treatment of samples required for TPD analyses. As we already noticed a decrease of basicity by XPS and Boehm titration after the heat treatment of EDA-AC or EDA-GNP, this pre-treatment at 850 °C could also have the same impact but the type of functions should not be much different. Nevertheless, it can be firmly concluded that the sample contains basic sites that are stable at temperatures up to 200 °C. A

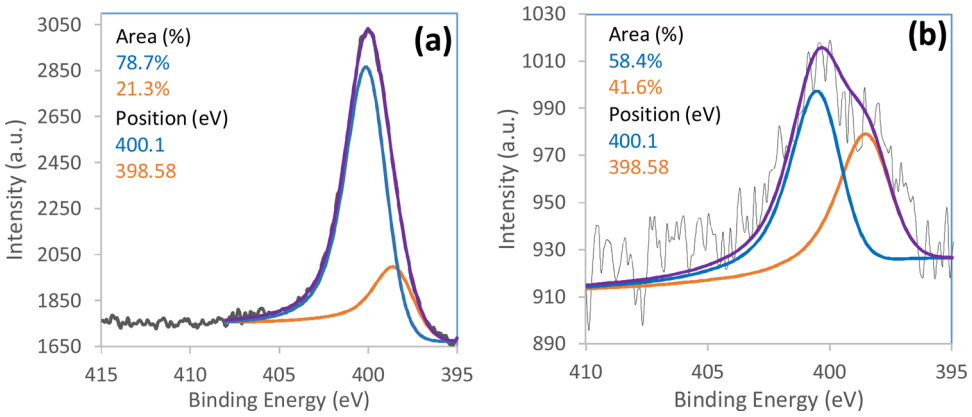

Fig. 2. N1s peaks (in blue: amine; in orange: pyridine/pyrrole) from XPS analyses of (a) N-doped GNP before heat-treatment (b) N-doped GNP after heat treatment at 900 °C, as a representative example (For interpretation of the references to colour in this figure legend, the reader is referred to the web version of this article).

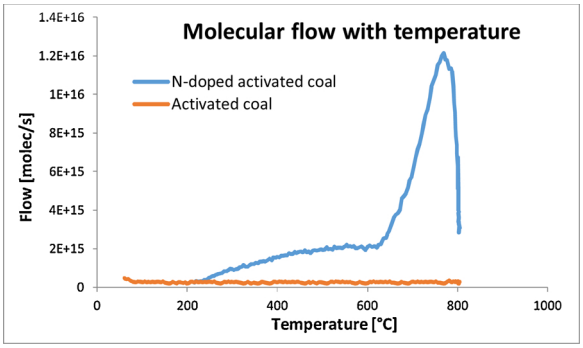

Fig. 3. Molecular flow of CO_2 as a function of the temperature for activated coal and N-doped activated coal.

higher stability is not needed as biomass transformation is carried out in water and thus never exceeds this limit.

3.3. Ru nanoparticles deposition on N-doped carbon supports

N-doped carbon materials were then used as supports for Ru nanoparticles. The nitrogen within the structure should help to reach good dispersion and a better tethering of the metal nanoparticles. The Ru nanoparticles were deposited on the supports with the precipitation/deposition method, as described in the experimental section and implemented on non-functionalized supports (Section 3.1). ICP analyses have confirmed that between 2.6 and 2.9 wt% of Ru were deposited on the supports (S7 in SI).

It is shown that the heat treatment used for reducing Ru nanoparticles has a slight influence on the nitrogen content and the types of nitrogen functions present in the final activated materials. It can be seen that the ratio of pyridine/pyrrole functions over amine functions is getting a bit higher after Ru deposition (S8 in SI). Indeed, the change in the type of nitrogen functions present is also depending on the duration of the heat treatment. As the N-doped carbon supports had already been heated beforehand up to 900 °C, the further treatment at 600 °C for Ru reduction will influence the nitrogen functions less dramatically than if it was the sole heat-treatment. This change in the composition of nitrogen functions would have been more substantial if the second heat treatment was done at a higher temperature than the first one. Heat treatment for the reduction of Ru nanoparticles has been optimized for each support in order to obtain a Ru nanoparticle size of $1-2$ nm. The catalysts on N-doped activated coal have been heated at 600 °C under Ar/H_2 (95/5) whereas the catalysts on N-doped GNP have been heated at 400 °C under Ar/H_2 (95/5). TEM images of these catalysts are presented in Fig. 4. We notice here that the Ru nanoparticles are better dispersed on the N-doped materials than on the pristine support (see section 3.1) showing the positive impact of the nitrogen presence within the lattice.

All catalysts were analyzed by XPS (S9 in SI) and the position of the $Ru_{3p3/2}$ peak indicated that metallic Ru is always obtained after the heat treatment under Ar/H_2.

The Ru/N-doped AC and Ru/N-doped GNP samples were also characterized by XRD (Fig. 5). The peaks around 26° and 43° correspond to the graphitic domains (002 and 100 reflections, respectively) of the AC and the GNP carbonaceous materials [32–34]. The peak at 44° matches with metallic Ru [35]. There is no meaningful difference between the Ru/pristine AC and the Ru/N-doped AC. However, the Ru peak is more visible in the case of Ru/N-doped GNP compared to the Ru/pristine GNP, even if the Ru loading (as measured by ICP, see above) is similar in all cases, indicating that the Ru nanoparticles are more crystalline when they are supported on N-doped GNP. Indeed the presence of the nitrogen functions seem to play a role in the structuration of the nanoparticles.

Basicity of the Ru/N-doped GNP has been measured by Boehm titrations. The results can be found in Table 3. The drop of basicity observed after the addition of Ru nanoparticles can be explained either by the fact that Ru nanoparticles will block the access to some of the nitrogen functions or by the heat treatment implemented to reduce the Ru. Indeed, a decrease of basicity has been observed after a heat treatment on EDA-GNP or EDA-oxidized GNP (see above).

3.4. Hydrolysis of cellobiose into glucose with N-doped carbons

It is known that acidic functions are the most suitable active sites for the hydrolysis of cellobiose into glucose. However it has been shown that when the acidic functions are too weak or in too low quantities they have no influence on the hydrolysis of cellobiose [9]. Nevertheless, hydrolysis in general is a chemical reaction that can also be catalyzed by basic functions. Given that the N-doped carbons that we have prepared contain basic functions (amine, pyridine, pyrrole, *etc.*), they might present an activity for the hydrolysis of the β-1,4-glycosidic bond (see Scheme 1). Acid sites are usually used to catalyze such transformation, but basic functions could also fulfill this role. Therefore, we carried out some catalytic tests on the hydrolysis of cellobiose into glucose under nitrogen in the absence of Ru or H_2 (Table 4). The solvent used is water. Indeed cellobiose is soluble in it and we also need water as a reactant for the hydrolysis (S10 in SI).

It is shown that N-doped carbons (AC and GNP) with or without heat treatment does not improve the hydrolysis of cellobiose into glucose. Indeed the results obtained are not better than the catalytic test without any catalyst (blank). Only the N-doped GNP before heat treatment, with the dangling EDA, is slightly increasing the conversion

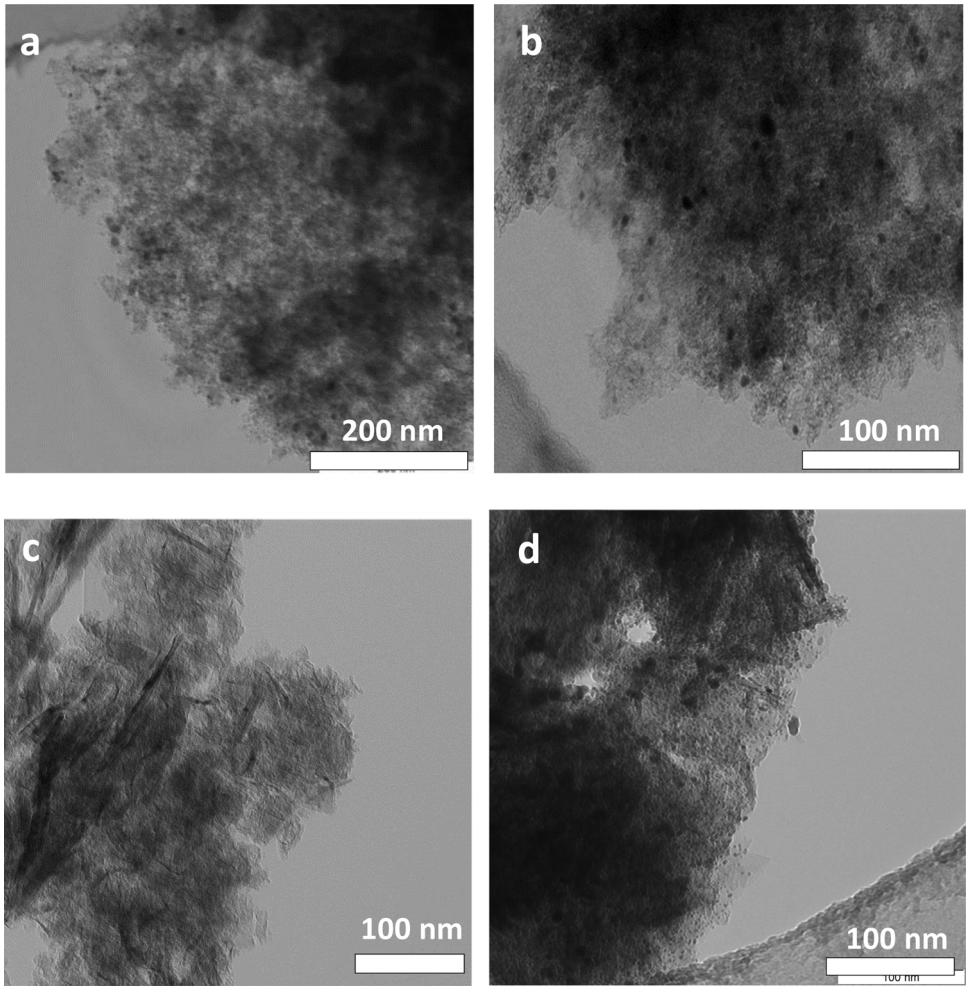

Fig. 4. TEM images of Ru nanoparticles on a) pristine AC ; b) N-doped AC ; c) pristine GNP ; d) N-doped GNP.

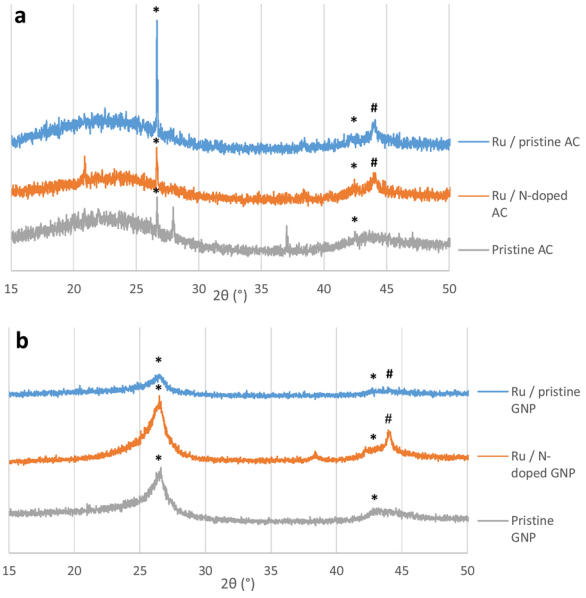

Fig. 5. XRD pattern for (a) pristine AC, Ru nanoparticles on AC and Ru nanoparticles on N-doped AC and for (b) pristine GNP, Ru nanoparticles on GNP and Ru nanoparticles on N-doped GNP. Asterisks denote peaks attributed to carbon phases and '#' denote Ru metal phase.

Table 3
Basicity of the GNP before and after deposition of Ru nanoparticles.

Catalysts	Basicity (mmol/100 g)
GNP	31
N-doped GNP	61
Ru / N-doped GNP	28
Oxidized GNP	0
N-doped oxidized GNP	81
Ru / N-doped oxidized GNP	35

but the selectivity towards glucose is lower. After the heat treatment, the N-doped GNP is giving the same results as the blank. The amount of basic functions on the carbon material should not be the issue, given that the molar ratio between cellobiose and basic functions is around 10 after heat treatment. The main explanation for this lack of activity is that the basic functions that have been introduced on the carbon supports are not adequate sites, given the mechanism [36], to catalyze the hydrolysis. We tested for comparison two modified carbon materials that display high acidity [9]. These catalysts have high activity for the hydrolysis unlike the N-doped carbon materials. Therefore, we can conclude that the nitrogen functions incorporated within the carbon supports will have no direct impact on the hydrolysis of cellobiose into glucose.

Table 4
Hydrolysis of cellobiose into glucose (160 °C; 1700 rpm; N_2; 2 h).

Catalyst	Conversion (%)	Selectivity in glucose (%)	Yield in glucose (%)
Blank (no catalyst)	42	70	29
AC pristine	43	60	26
N doped AC before heat treatment	33	61	20
N doped AC after heat treatment	38	59	22
GNP pristine	43	68	29
N doped GNP before heat treatment	57	33	19
N doped GNP after heat treatment	37	73	27
SO_3H on AC [1]	86	86	74
SO_3H on GNP [1]	93	84	78

[1] Results with catalysts from [9].

3.5. Hydrogenation of cellobiose into sorbitol

The previous section indicated that the basic functions are not playing an active and direct role in the hydrolysis of cellobiose into glucose. Therefore, we can reach our final goal and assess the impact of nitrogen functions on the activity of Ru nanoparticles for the direct transformation of cellobiose into sorbitol. We selected, for this part of the work, the most promising catalysts among the materials synthesized in the previous sections, to assess their activity in this 2-step transformation. Kinetic curves have been built over 6 h period for four representative catalysts (Fig. 6). As mentioned in the introduction, two pathways are possible to obtain sorbitol from cellobiose. The same reaction pattern is observable in all cases. Indeed the preferential pathway is going through the hydrogenation of cellobiose into cellobitol before breaking this hydrogenated disaccharide into sorbitol/glucose (see Scheme 1 in Introduction). After 1 – 2 hours, cellobitol production is reaching a peak before decreasing. Concomitantly, sorbitol production rises. A very peculiar observation is that nearly no glucose accumulation has been observed during the course of the reaction. This means that as soon as the glucose is formed by cellobitol hydrolysis, it is hydrogenated into sorbitol. It is confirming, as mentioned in literature [37], that both hydrogenation reactions are faster than the two hydrolysis steps (see above Scheme 1).

We notice that both catalysts prepared on N-doped supports display better activity than the catalysts on non-functionalized supports (Table 5). This is the proof that the nitrogen atoms incorporated in the lattice enhance the Ru nanoparticles activity.

This can be explained first by the fact that the nitrogen atoms improved the dispersion of the Ru nanoparticles (see TEM images and discussion above). Second, they can also influence the spin density and the charge distribution, which have an impact on the Ru reactivity as already shown in the literature [24]. Unfortunately, we could not detect

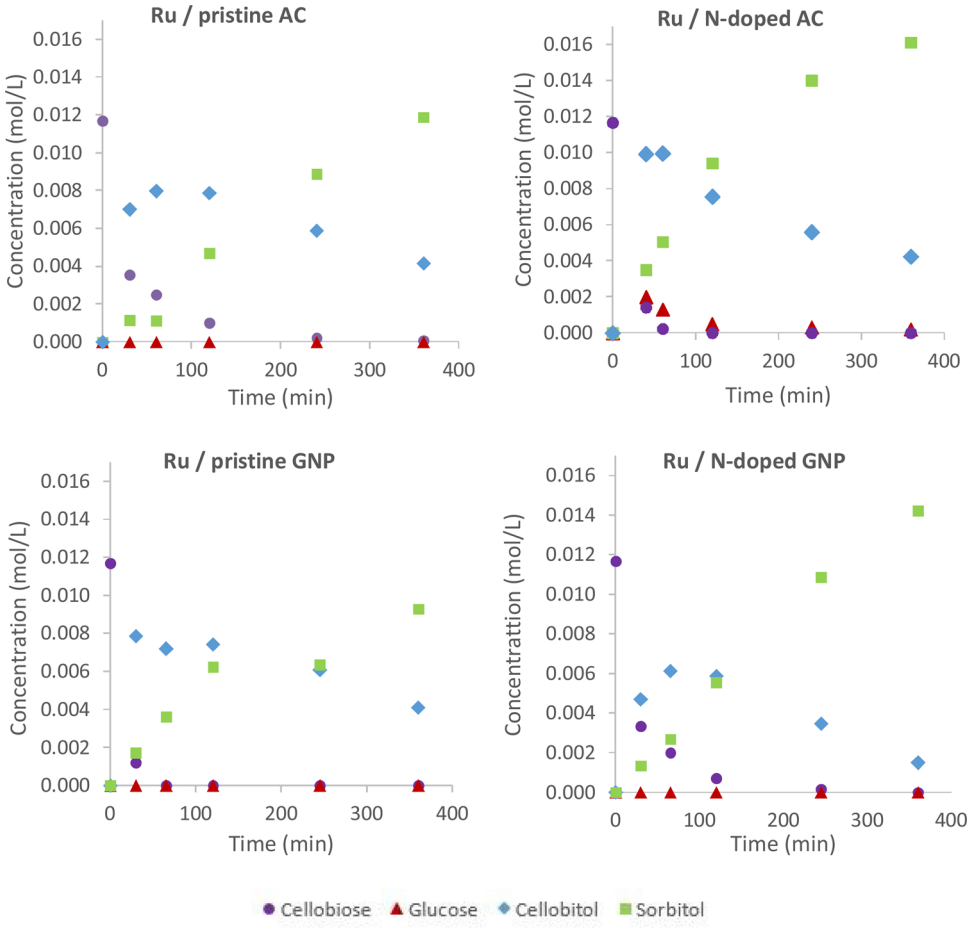

Fig. 6. Kinetic curves for the transformation of cellobiose into sorbitol (testing conditions: 160 °C; 30 bar H_2; 1700 rpm).

Table 5
Hydrogenation of cellobiose into sorbitol with pristine and N-doped AC and GNP: conversion of cellobiose and selectivity into glucose, cellobitol and sorbitol after 6 h (160 °C; 1700 rpm; 30 bar H_2).

Catalyst	Conversion (%)	Selectivity in glucose (%)	Selectivity in cellobitol (%)	Selectivity in sorbitol (%)	Yield in sorbitol (%)
Ru / pristine AC	99	0	36	51	51
Ru / pristine GNP	100	0	35	40	40
Ru / N-doped AC	100	1	31	66	66
Ru / N-doped GNP	100	0	13	61	61

Table 6
Hydrogenation of cellobiose into sorbitol without catalyst (blank), with N-doped GNP, EDA GNP and with a mixture of Ru/GNP and N-doped GNP: conversion of cellobiose, selectivity into glucose, cellobitol and sorbitol and yield in sorbitol after 2 h (160 °C; 1700 rpm; 30 bar H_2).

Catalyst	Conversion (%)	Selectivity in glucose (%)	Selectivity in cellobitol (%)	Selectivity in sorbitol (%)	Yield in sorbitol (%)
Blank	21	52	0	0	0
Ru / N-doped GNP	95	6	50	29	28
Ru / EDA GNP	70	0	57	11	8
Ru / GNP + N-doped GNP (mechanical mix)	100	0	64	22	22

any by-product apart from some traces of fructose (produced by isomerization of glucose). It is known that 5-HMF or levulinic acid could be obtained as products from degradation of sorbitol but their presence could not be confirmed with our HPLC system. Therefore, total organic content (TOC) analyses were performed and it was confirmed that the carbon balance at the end of the reaction in solution was respected (S11 in SI).

Some catalytic tests have been performed with Ru nanoparticles on EDA GNP as support (Table 6). In this case the nitrogen has not been incorporated into the carbon lattice and mainly ethylenediamine NH_2 dangling functions are present. The results have shown that this catalyst is less active than the bifunctional catalyst Ru / N-doped GNP. A mechanical mixture between Ru / GNP and N-doped GNP has also been tested. As this mixture is less active than the bifunctional catalyst, it proves that the Ru nanoparticles have to be on the N-doped support to be promoted by the nitrogen functions. A simple proximity between the two type of solids is not enough to enhance the Ru activity.

Recyclability tests have been performed with the Ru/N-doped GNP catalyst to assess the stability of the catalyst over several runs. After each catalytic test, the catalyst was recovered and dried. It has then be reused for the next reaction. The results are shown in Table 7 for a total of three consecutive catalytic tests. We can see that the conversion remains the same in all the different runs. The selectivity is slightly lower for the 2nd and the 3rd run. Despite this slight decrease of selectivity after the first reaction, the catalyst can be re-used for many runs without losing its activity.

XPS analyses and TEM images have been carried out on the used catalyst (S12 and S13 in SI). These analyses have confirmed that the used catalyst has quite the same composition and morphology than the starting catalyst. XPS analyses have indicated that the nitrogen functions have the same composition than before the catalytic tests. TEM images have shown that Ru nanoparticles have the same size and the same dispersion on the support, confirming the stability of our bifunctional material.

By improving the Ru hydrogenation ability, we have promoted sorbitol formation from cellobiose without requiring hydrolysis secondary active sites or the addition of inorganic acids in the solution. This opens the door to many applications for biomass valorization reactions that currently still depend on environmentally harmful substances.

4. Conclusion

Three different carbon supports, namely carbon nanofibers, activated coal and graphene nanoplatelets have been modified to incorporate nitrogen atoms within the lattice of the carbon sheets. These N-doped carbon materials have been analyzed by XPS, TPD and Boehm titration, which demonstrated successful modification, thereby increasing surface basicity and number of pyridine/pyrrole sites. These new supports were used to deposit Ru nanoparticles. TEM and XRD analyses have shown improvement of the deposition of Ru nanoparticles on N-doped carbon supports compared with the pristine ones. The nanoparticles are better dispersed and more crystalline.

These Ru/N-doped carbon catalysts have been tested for the direct 2-steps transformation of cellobiose into sorbitol. Optimal Ru nanoparticles size for the hydrogenation of glucose into sorbitol were first determined to be around $1-2$ nm. Then, the impact of the nitrogen functions on cellobiose hydrolysis was assessed as null. Kinetic curves for the full transformation have demonstrated that the first step is the hydrogenation of cellobiose into cellobitol and the second step is cellobitol hydrolysis into one molecule of sorbitol and one molecule of glucose that is directly transformed into sorbitol. This study clearly highlighted the better activity of the catalysts supported on N-doped carbon materials compared to pristine ones. Nitrogen within the structure of the support is improving the Ru nanoparticles activity. Finally, one of our best catalysts has been tested several times to assess its recyclability. It displayed high activity over several runs showing that neither the introduced nitrogen functions nor the Ru nanoparticles suffer from deactivation, as confirmed by XPS and TEM analyses.

CRediT authorship contribution statement

Samuel Carlier: Methodology, Validation, Investigation, Writing - original draft, Visualization. **Jim Gripekoven:** Investigation. **Martin**

Table 7
Recyclability tests of the Ru/N-doped GNP; conversion of cellobiose, selectivity in sorbitol and yield in sorbitol after 2 h (160 °C; 1700 rpm; 30 bar H_2).

Catalyst	Conversion (%)	Selectivity in sorbitol (%)	Yield in sorbitol (%)
Ru/N-doped GNP 1st run	95	29	28
Ru/N-doped GNP 2nd run	95	23	22
Ru/N-doped GNP 3rd run	96	23	22

Philippo: Investigation. **Sophie Hermans:** Conceptualization, Methodology, Resources, Writing - review & editing, Supervision, Project administration, Funding acquisition.

Declaration of Competing Interest

The authors report no declarations of interest.

Acknowledgments

The authors wish to thank the Fonds de la Recherche Scientifique (F.R.S. – FNRS) and the Université catholique de Louvain (Belgium) for funding. We are grateful to Jean François Statsyns for lab technical assistance, Pierre Eloy for XPS analyses, François Devred for TPD and XRD analyses, Laurent Collard for HPLC technical assistance, Claudine Givron for the TOC analyses and Anne Iserentant for the ICP analyses.

Appendix A. Supplementary data

Supplementary material related to this article can be found, in the online version, at doi:https://doi.org/10.1016/j.apcatb.2020.119515.

References

[1] R. Parajuli, T. Dalgaard, U. Jørgensen, A.P.S. Adamsen, M.T. Knudsen, M. Birkved, M. Gylling, J.K. Schjørring, Biorefining in the prevailing energy and materials crisis: a review of sustainable pathways for biorefinery value chains and sustainability assessment methodologies, Renewable Sustainable Energy Rev. 43 (2015) 244–263, https://doi.org/10.1016/j.rser.2014.11.041.

[2] A.M. Ruppert, K. Weinberg, R. Palkovits, Hydrogenolysis goes bio: from carbohydrates and sugar alcohols to platform chemicals, Angew. Chem. Int. Ed. 51 (2012) 2564–2601, https://doi.org/10.1002/anie.201105125.

[3] M. Sarra, T. Rouissi, S.K. Brar, J.F. Blais, Life cycle analysis of potential substrates of sustainable biorefinery, Platf. Chem. Biorefinery (2016) 55–76, https://doi.org/10.1016/b978-0-12-802980-0.00004-3.

[4] A. Fukuoka, P.L. Dhepe, Catalytic conversion of cellulose into sugar alcohols, Angew. Chem. Int. Ed. 45 (2006) 5161–5163, https://doi.org/10.1002/anie.200601921.

[5] V. Gitifar, R. Eslamloueyan, M. Sarshar, Experimental study and neural network modeling of sugarcane bagasse pretreatment with H2SO4 and O3 for cellulosic material conversion to sugar, Bioresour. Technol. 148 (2013) 47–52, https://doi.org/10.1016/j.biortech.2013.08.060.

[6] A. Onda, T. Ochi, K. Yanagisawa, Selective hydrolysis of cellulose into glucose over solid acid catalysts, Green Chem. 10 (2008) 1033–1037, https://doi.org/10.1039/b808471h.

[7] S. Suganuma, K. Nakajima, M. Kitano, D. Yamaguchi, H. Kato, S. Hayashi, M. Hara, Hydrolysis of cellulose by amorphous carbon bearing SO3H, COOH, and OH groups, J. Am. Chem. Soc. 130 (2008) 12787–12793, https://doi.org/10.1021/ja803983h.

[8] J.M.A.R. Almeida, L. Da Vià, P. Demma Carà, Y. Carvalho, P.N. Romano, J.A.O. Peña, L. Smith, E.F. Sousa-Aguiar, J.A. Lopez-Sanchez, Screening of mono- and bi-functional catalysts for the one-pot conversion of cellobiose into sorbitol, Catal. Today 279 (2017) 187–193, https://doi.org/10.1016/j.cattod.2016.06.017.

[9] S. Carlier, S. Hermans, Highly efficient and recyclable catalysts for cellobiose hydrolysis: systematic comparison of carbon nanomaterials functionalized with benzyl sulfonic acids, Front. Chem. 8 (2020) 1–9, https://doi.org/10.3389/fchem.2020.00347.

[10] L.K. Tolonen, M. Bergenstråhle-Wohlert, H. Sixta, J. Wohlert, Solubility of cellulose in supercritical water studied by molecular dynamics simulations, J. Phys. Chem. B 119 (2015) 4739–4748, https://doi.org/10.1021/acs.jpcb.5b01121.

[11] N.P. Novoselov, E.S. Sashina, V.E. Petrenko, M. Zaborsky, Study of dissolution of cellulose in ionic liquids by computer modeling, Fibre Chem. 39 (2007) 153–158, https://doi.org/10.1007/s10692-007-0030-y.

[12] M. Yabushita, H. Kobayashi, A. Fukuoka, Catalytic transformation of cellulose into platform chemicals, Appl. Catal. B Environ. 145 (2014) 1–9, https://doi.org/10.1016/j.apcatb.2013.01.052.

[13] C. Marques, R. Tarek, M. Sara, S.K. Brar, Sorbitol production from biomass and its global market, Platf. Chem. Biorefinery (2016) 217–227, https://doi.org/10.1016/b978-0-12-802980-0.00012-2.

[14] L. Negahdar, J.U. Oltmanns, S. Palkovits, R. Palkovits, Kinetic investigation of the catalytic conversion of cellobiose to sorbitol, Appl. Catal. B Environ. 147 (2014) 677–683, https://doi.org/10.1016/j.apcatb.2013.09.046.

[15] N. Yan, C. Zhao, C. Luo, P.J. Dyson, H. Liu, Y. Kou, One-step conversion of cellobiose to C6-alcohols using a ruthenium nanocluster catalyst, J. Am. Chem. Soc. 128 (2006) 8714–8715, https://doi.org/10.1021/ja062468t.

[16] C. Luo, S. Wang, H. Liu, Cellulose conversion into polyols catalyzed by reversibly formed acids and supported ruthenium clusters in hot water, Angew. Chem. Int. Ed. 46 (2007) 7636–7639, https://doi.org/10.1002/anie.200702661.

[17] W. Zhu, H. Yang, J. Chen, C. Chen, L. Guo, H. Gan, X. Zhao, Z. Hou, Efficient hydrogenolysis of cellulose into sorbitol catalyzed by a bifunctional catalyst, Green Chem. 16 (2014) 1534–1542, https://doi.org/10.1039/c3gc41917g.

[18] G. Liang, L. He, H. Cheng, W. Li, X. Li, C. Zhang, Y. Yu, F. Zhao, The hydrogenation/dehydrogenation activity of supported Ni catalysts and their effect on hexitols selectivity in hydrolytic hydrogenation of cellulose, J. Catal. 309 (2014) 468–476, https://doi.org/10.1016/j.jcat.2013.10.022.

[19] H. Wang, J. Lv, X. Zhu, X. Liu, J. Han, Q. Ge, Efficient hydrolytic hydrogenation of cellulose on mesoporous HZSM-5 supported Ru catalysts, Top. Catal. 58 (2015) 623–632, https://doi.org/10.1007/s11244-015-0409-6.

[20] A. Negoi, K. Triantafyllidis, V.I. Parvulescu, S.M. Coman, The hydrolytic hydrogenation of cellulose to sorbitol over M (Ru, Ir, Pd, Rh)-BEA-zeolite catalysts, Catal. Today 223 (2014) 122–128, https://doi.org/10.1016/j.cattod.2013.07.007.

[21] P.A. Lazaridis, S.A. Karakoulia, C. Teodorescu, N. Apostol, D. Macovei, A. Panteli, A. Delimitis, S.M. Coman, V.I. Parvulescu, K.S. Triantafyllidis, High hexitols selectivity in cellulose hydrolytic hydrogenation over platinum (Pt) vs. ruthenium (Ru) catalysts supported on micro/mesoporous carbon, Appl. Catal. B Environ. 214 (2017) 1–14, https://doi.org/10.1016/j.apcatb.2017.05.031.

[22] W. Deng, M. Liu, X. Tan, Q. Zhang, Y. Wang, Conversion of cellobiose into sorbitol in neutral water medium over carbon nanotube-supported ruthenium catalysts, J. Catal. 271 (2010) 22–32, https://doi.org/10.1016/j.jcat.2010.01.024.

[23] W. Deng, X. Tan, W. Fang, Q. Zhang, Y. Wang, Conversion of cellulose into sorbitol over carbon nanotube-supported ruthenium catalyst, Catal. Lett. 133 (2009) 167–174, https://doi.org/10.1007/s10562-009-0136-3.

[24] D. Wei, Y. Liu, Y. Wang, H. Zhang, L. Huang, G. Yu, Synthesis of n-doped graphene by chemical vapor deposition and its electrical properties, Nano Lett. 9 (2009) 1752–1758, https://doi.org/10.1021/nl803279t.

[25] P.J.C. Hausoul, L. Negahdar, K. Schute, R. Palkovits, Unravelling the Ru-catalyzed hydrogenolysis of biomass-based polyols under neutral and acidic conditions, ChemSusChem 8 (2015) 3323–3330, https://doi.org/10.1002/cssc.201500493.

[26] Y. Niu, H. Wang, X. Zhu, Z. Song, X. Xie, X. Liu, J. Han, Q. Ge, Ru supported on zirconia-modified SBA-15 for selective conversion of cellobiose to hexitols, Microporous Mesoporous Mater. 198 (2014) 215–222, https://doi.org/10.1016/j.micromeso.2014.07.030.

[27] H.-P. Boehm, E. Diehl, W. Heck, R. Sappok, Surface oxides of carbon, Angew. Chem. Int. Ed. Engl. 3 (1964) 669–677, https://doi.org/10.1002/anie.196406691.

[28] S.L. Goertzen, K.D. Thériault, A.M. Oickle, A.C. Tarasuk, H.A. Andreas, Standardization of the Boehm titration. Part I. CO2 expulsion and endpoint determination, Carbon 48 (2010) 1252–1261, https://doi.org/10.1016/j.carbon.2009.11.050.

[29] T. Haynes, V. Dubois, S. Hermans, Particle size effect in glucose oxidation with Pd/CB catalysts, Appl. Catal. A Gen. 542 (2017) 47–54, https://doi.org/10.1016/j.apcata.2017.05.008.

[30] J.A. Menéndez, J. Phillips, B. Xia, L.R. Radovic, On the modification and characterization of chemical surface properties of activated carbon: in the search of carbons with stable basic properties, Langmuir 12 (1996) 4404–4410, https://doi.org/10.1021/la9602022.

[31] C. Breyer, D. Reichert, J. Seidel, R. Hüttl, F. Mertens, S. Kureti, Kinetic modeling of the adsorption and desorption of CO 2 on α-Fe 2 O 3, Phys. Chem. Chem. Phys. 17 (2015) 27011–27018, https://doi.org/10.1039/C5CP04671H.

[32] R. Siburian, H. Sihotang, S. Lumban Raja, M. Supeno, C. Simanjuntak, New route to synthesize of graphene nano sheets, Orient. J. Chem. 34 (2018) 182–187, https://doi.org/10.13005/ojc/340120.

[33] K.L. Routray, S. Saha, D. Behera, Nanosized CoFe2O4-graphene nanoplatelets with massive dielectric enhancement for high frequency device application, Mater. Sci. Eng. B Solid-State Mater. Adv. Technol. 257 (2020) 114548, , https://doi.org/10.1016/j.mseb.2020.114548.

[34] Z.Q. Li, C.J. Lu, Z.P. Xia, Y. Zhou, Z. Luo, X-ray diffraction patterns of graphite and turbostratic carbon, Carbon 45 (2007) 1686–1695, https://doi.org/10.1016/j.carbon.2007.03.038.

[35] J.Z. Bloh, R. Dillert, D.W. Bahnemann, Ruthenium-modified zinc oxide, a highly active vis-photocatalyst: the nature and reactivity of photoactive centres, Phys. Chem. Chem. Phys. 16 (2014) 5833–5845, https://doi.org/10.1039/c3cp55136a.

[36] G.W. Huber, S. Iborra, A. Corma, Synthesis of transportation fuels from biomass: chemistry, catalysts, and engineering, Chem. Rev. 106 (2006) 4044–4098, https://doi.org/10.1021/cr068360d.

[37] P.J.C. Hausoul, A.K. Beine, L. Neghadar, R. Palkovits, Kinetics study of the Ru/C-catalysed hydrogenolysis of polyols-insight into the interactions with the metal surface, Catal. Sci. Technol. 7 (2017) 56–63, https://doi.org/10.1039/c6cy02104b.